coatings

MDPI

Article

Study of Ceramic Hollow Buoyant Balls Prepared Based on Slip Mold Casting and Brazing Process

Yu Lei [1], Jian Zhou [1,*], Guizhen Liu [1], Lin Wang [1] and Zhongjun Ding [2]

[1] State Key Laboratory of Advanced Technology for Materials Synthesis and Processing, Wuhan University of Technology, Wuhan 430070, China; lydsg894666012@163.com (Y.L.); gzliu66@126.com (G.L.); lin_wang@whut.edu.cn (L.W.)
[2] National Deep Sea Center, Qingdao 266237, China; dzj@ndsc.org.cn
* Correspondence: jianzhou@whut.edu.cn

Abstract: In the domain of deep-sea buoyancy material applications, hollow ceramic spheres, known for their high strength and low mass-to-drainage ratio, contribute to increased buoyancy and payload capacity enhancement for deep submersibles, constituting buoyancy materials of exceptional overall performance. This study entails the brazing of two ceramic hemispherical shells, obtained through slurry molding, to form a ceramic float. This process, which integrates slurry molding and ceramic brazing, facilitates buoyancy provision. Further refinement involves welding a ceramic connector onto the ceramic shell, incorporating a top opening to create a ceramic float equipped with an observation window seat. The ceramic float maintains uniform wall thickness, while the observation window facilitates external environmental observation in deep-sea research. Two pressure-resistant spherical shells, produced using this process, underwent testing, revealing the wall thickness of the prepared alumina ceramic hollow spheres to be 1.00 mm, with a mass-to-drainage ratio of 0.47 g/cm^3 and a buoyancy coefficient of 53%. The resultant ceramic hollow floating ball can withstand hydrostatic pressure of 120 MPa, while the pressure-resistant ball shell with an observation window seat can endure hydrostatic pressure of 100 MPa, ensuring safe operation at depths of 5000–6000 m. This process provides a production method for subsequent large-scale ceramic float manufacturing for the transportation of objects or personnel.

Keywords: static slip casting; welding; ceramic hollow floating ball; viewing window holder

Citation: Lei, Y.; Zhou, J.; Liu, G.; Wang, L.; Ding, Z. Study of Ceramic Hollow Buoyant Balls Prepared Based on Slip Mold Casting and Brazing Process. *Coatings* **2024**, *14*, 767. https://doi.org/10.3390/coatings14060767

Academic Editors: Oana Catalina Mocioiu and Ana-Maria Mocioiu

Received: 7 May 2024
Revised: 13 June 2024
Accepted: 13 June 2024
Published: 17 June 2024

1. Introduction

As terrestrial resources diminish, the exploitation of seabed resources emerges as a prominent trend. However, ocean exploration encounters significant challenges, including exceptionally high water pressure, limited visibility, and harsh environmental conditions [1]. Hence, the development of deep-sea resources hinges on the research and fabrication of underwater operational equipment, with buoyant materials assuming a crucial role in this endeavor [2]. Hollow ceramic spheres, serving as buoyancy materials, exhibit high strength and low mass–drainage ratios, thereby enhancing buoyancy and augmenting the payload capacity of deep submergence vehicles, rendering them buoyancy materials of exceptional overall performance. The prevailing method for preparing buoyancy balls primarily involves the 3D printing of hemispherical shells, followed by sealed sintering [3]. Nevertheless, 3D-printed molded ceramic hemispherical shells often exhibit uneven shrinkage and variations in wall thickness gradients. Furthermore, these methods necessitate the use of carbon fiber to seal the sintered clamping surface, thereby escalating costs and susceptibility to breakage [4]. In conclusion, there exists a necessity to further refine and optimize the preparation methods of ceramic hollow buoyancy spheres to align with the requirements of deep-sea equipment [5,6]. Slip casting plays a crucial role in the production of ceramic hollow buoyancy spheres. It facilitates the creation of intricate shapes and precise dimensions by pouring a ceramic slurry into a porous mold, allowing

the water to be absorbed, leaving a solid ceramic shell. This method enables the formation of hollow interiors, which are essential for buoyancy spheres, as they need to be lightweight while maintaining structural integrity. The conventional ceramic molding process involves casting ceramic slurry into plaster molds, serving as a current method for shaping thin-walled ceramic components [7]. However, prototyping complex parts entails the creation of multiple designs and the manufacturing of molds, dies, fixtures, and other necessary components [8]. Simultaneously, the gypsum molds are prone to degradation, leading to extended production times and necessitating specific storage requirements, resulting in irregularly shaped castings that are susceptible to disintegration during demolding [9]. Relying solely on slip casting proves to be a costly approach for mass-producing ceramic floats or ceramic pressure-resistant housing assemblies. Thus, when substantial quantities of these components are needed, the initial production involves creating simple ceramic structures, which are subsequently assembled or bonded together to form the ceramic housings [10,11].

Currently, ceramic connection methods primarily comprise adhesive bonding and metallurgical bonding. The adhesive bonding method offers advantages such as a straightforward process and high efficiency [12]. Nevertheless, the colloids utilized for bonding exhibit a low melting point, leading to diminished strength and inadequate airtightness of the joint [13]. Active brazing stands as a widely adopted technique for joining ceramics, offering an effective means to attain high-quality and durable ceramic bonds [14]. The discontinuity of the material leads to an increased local stress concentration in the ceramic connection. Excessive local stress is more likely to induce crack propagation, rendering the connection vulnerable to rupture and resulting in shell breakage. Hence, it is imperative to select an appropriate connection process for molding the ceramic float. The significance of brazing in the preparation process of ceramic hollow floating balls lies in its role as a bonding method for joining ceramic components. Brazing ensures structural integrity and seals the hollow interiors, enhancing the overall performance and durability of the floating balls. By heating a filler metal, typically a brazing alloy, to its melting point and flowing it into the joint between ceramic parts, brazing forms a strong metallurgical bond upon cooling. This process facilitates the assembly of complex ceramic structures with precise geometries [13,15].

In this experiment, a combination of the slip casting process and welding process is employed. Initially, two ceramic hemispherical shells are prepared using the slip casting method, followed by the welding together of these two ceramic hemispherical shells using brazing material [16]. Following high-temperature sintering to acquire alumina ceramic hollow floats, the hemispherical shell allows for better control of wall thickness uniformity. Additionally, isostatic pressing of ceramic hemispherical shell blanks can be performed to enhance the mechanical strength of the sintered floats [17]. A ceramic pressure-resistant spherical shell with an opening at the upper end is fabricated via slip casting, following which a ceramic connector is soldered to serve as a viewing window for the pressure-resistant spherical shell [18]. The study investigated the impact of the solid content of the ceramic slurry and the concentration of the added dispersant on the viscosity of the ceramics during the slip casting process. Additionally, the microscopic morphology of the ceramic sintered specimens was examined at various sintering temperatures to ascertain the optimal sintering process [19]. During the soldering process, the phase compositions of the braze–ceramic solder interface were analyzed using X-ray diffraction at different temperatures, aiming to identify the optimum soldering temperature. Additionally, the shear strength of the soldered specimens was assessed. Furthermore, different mass fractions of CuO powder were incorporated as wetting additives to the existing brazing material at the determined optimal welding temperature, and the shear strength of the weld specimens was evaluated [20]. To prevent the implosion of the float due to excessive pressure in the deep sea [21,22], in this study, pressure-holding tests and cyclic pressurization of molded ceramic floats were conducted to showcase the pressure resistance of the tested ceramic floats under high-pressure conditions. This substantiates the reliability of the process

for preparing pressure-resistant spherical shells by integrating slip casting and welding processes [23,24].

This experiment utilizes a combination of slip casting and brazing processes. It involves molding two ceramic hemispherical shells and subsequently brazing and sealing them to form a ceramic hollow floating ball. In comparison to the traditional method of molding a complete ceramic hollow float, the static slurry molding of hemispherical shells results in a more uniform wall thickness than molding the entire ceramic billet.

Simultaneously, the forming and sintering times for the ceramic hemispherical shells are shorter, greatly enhancing production efficiency and cost-effectiveness. In contrast to previous monolithic molding techniques for ceramic floats, this experiment involves brazing a connector at the open end of the ceramic float. This connector acts as an observation window, facilitating deep-sea observation, and offers an experimental foundation for future development of a connection channel for larger manned and cargo-carrying hollow floats. This molding process substantially improves the functionality of ceramic hollow floats.

2. Materials and Methods

2.1. Alumina Ceramic Hollow Dome Shell Size Design

The design sketch of the ceramic hemisphere shell utilized in this experiment is depicted in Figure 1. Subsequent sintering experiments are anticipated to yield a wall thickness of merely 1 mm for the hemispherical shell, with an additional thickness of 1.2 mm near the bonding surface. Hemispherical shell diameter is 48 mm. Augmenting the thickness of the hemispherical outer shell in the equatorial region serves to increase the contact area for welding while minimizing deformation effects on the circular welding surface, thereby enhancing the safety factor of the joint.

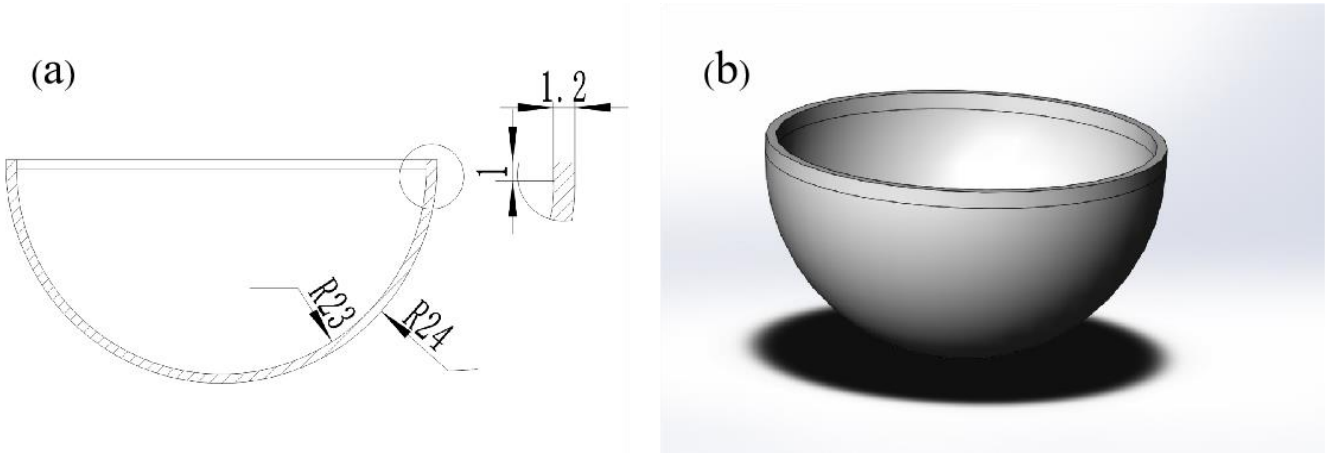

Figure 1. Technical sketch of the hemispherical housing. (**a**) CAD drawing; (**b**) 3D model.

2.2. Pressure-Resistant Spherical Shell Design with Viewing Window Holder

Ceramic hollow floating spheres are formed by welding two ceramic hemisphere shells, albeit welding in the equatorial plane results in a lengthy weld seam. The length of this seam significantly impacts the welding performance. To mitigate this, and to accommodate additional items necessary for deep-sea research or transporting researchers, ceramic sphere shells with open tops can first be injection molded. These shells then serve as observation window holders for the pressure-resistant sphere shells, achieved by welding ceramic connectors, as depicted in Figure 2a. The ceramic hollow float measures 48 mm in diameter, with a top opening diameter of 10 mm. The connector has an outer diameter of 13 mm and an inner diameter of 10 mm. Furthermore, the top welded ceramic connector can be replaced with a ceramic flange, facilitating the connection between the pressure-resistant spherical shell and the deep submersible via flange, as illustrated in Figure 2b.

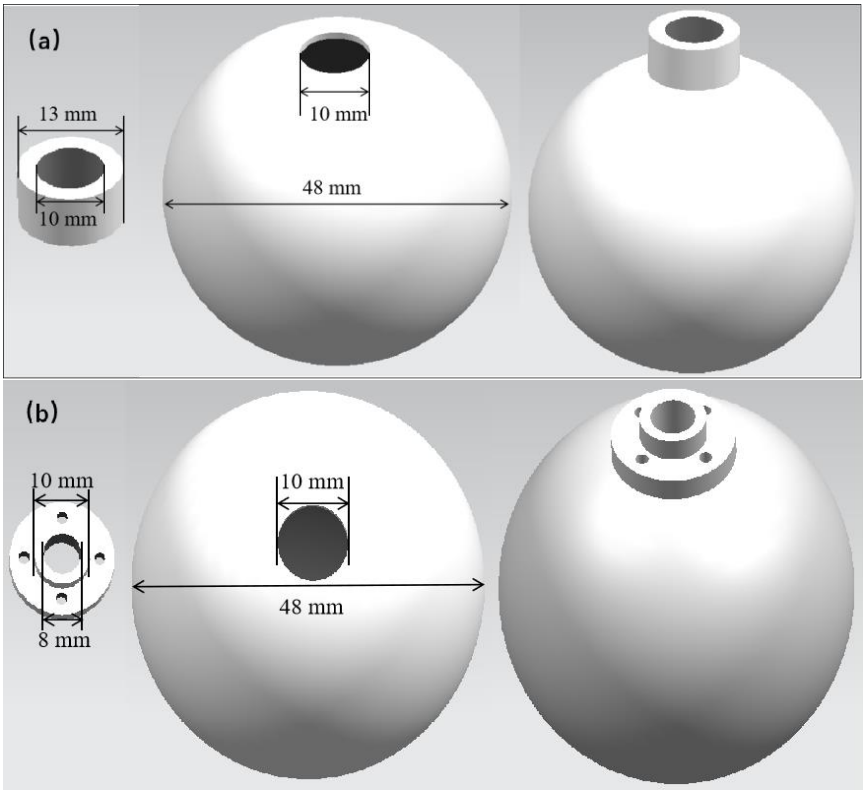

Figure 2. Two kinds of ceramic floats. (**a**) Ceramic float with connector. (**b**) Ceramic float with flange.

2.3. Raw Materials

The slurry used in the rotary grouting process consists of a solid phase and a liquid phase; the solid phase is mainly alumina powder (99.99%, Sinopharm Chemical Reagent Co., Ltd., Shanghai, China), and the liquid phase is deionized water. Ammonium polyacrylate (40% in water, Sinopharm Chemical Reagent Co., Ltd., China) (40% in water, Sinopharm Chemical Reagent Co., Ltd., China) and ammonia (AR, Sinopharm Chemical Reagent Co., Ltd., China) were used as dispersants and pH adjusters to reduce the viscosity of the slurry.

2.4. Preparation of Ceramic Slurry

The preparation of alumina slurry is a complex and dynamic process, involving several steps. Initially, 0.25 wt% of ammonium polyacrylate relative to alumina is dissolved in 30 g of deionized water. Then, a concentrated ammonia solution is slowly added to adjust the pH of the solution to 9.5. The resulting mixture is transferred to an ultrasonic cleaner for 10 min of ultrasonic treatment. Next, approximately 70 g of alumina powder is slowly added to the solution while stirring, ensuring that the solid content of the alumina particles remains within the range of 55–75 wt%. Lastly, the mixture was placed into a planetary ball mill with a material-to-ball ratio of 1:1.5 and stirred at 250 revolutions per minute for 2 h. This process yields a highly concentrated and evenly dispersed ceramic slurry.

2.5. Forming Method of Alumina Ceramic Floating Ball

Ceramic hollow floats for deep-sea applications are commonly produced through monolithic rotary slip casting. The high porosity and water absorption capacity of gypsum facilitate the deposition of slurry, leading to the formation of thin-walled intact hollow spherical shell blanks. However, the overall rotation during the slurry injection process fails to ensure uniform distribution of the slurry. This deficiency results in reduced wall thickness uniformity of the raw billet, impacting sphericity after sintering and diminishing the mechanical properties of the hollow spheres. Moreover, the irregular rotation method impedes mass production.

To avoid uneven wall thickness in the ceramic hollow float billets prepared for this experiment, two hemispherical ceramic shells were cast using the static slip casting method. The slurry was poured into a plaster mold and allowed to stand for 15–18 s. Unlike rotational molding, the static treatment ensured uniform adhesion of the slurry to the surface of the plaster mold, followed by draining out of excess slurry. Subsequently, the plaster molds were placed in a vacuum dryer and dried at 25 °C. The molds were then demolded to obtain raw unprocessed ceramic blanks. The processed raw shells were pre-fired in a muffle furnace at 1000 °C for two hours to prevent cracking of the raw ceramic spherical shells due to rapid heating and to improve the densification of the finished spherical shells. Finally, defect-free half-shell samples were sintered in a high-temperature silicon molybdenum furnace at 1600 °C for three hours under an air atmosphere.

2.6. Welding of Ceramic Ball Shells

The half-spherical shell specimens underwent a meticulous and progressive grinding process on an automatic grinder, utilizing silicon nitride water-abrasive papers with grit sizes ranging from 400# to 2000# [25]. Following the grinding process, the samples were polished using 2.5 μm diamond suspension fluid, followed by ultrasonic cleaning with alcohol and drying in a hot-air oven.

Subsequently, $Ag_{72}Cu_{28}$, the braze material, was evenly distributed on the ceramic half-spheres, which were subsequently assembled into ceramic balls for welding experiments. Similarly, the solder brazing material was evenly applied to the bottom of the ceramic connector and the opening of the ceramic ball housing to assemble a ceramic pressure-resistant ball housing with a flat circular window seat. The assembled sample was then positioned between two crucibles, with sufficient pressure applied to the upper crucible to ensure tight joining of the Al_2O_3 ceramic component coated with braze material during the brazing process.

The assembled sample was heated in a Mafu furnace with a ramp rate of 10 °C/min, reaching 800 °C and held for 10 min to ensure complete evaporation of organic compounds in the braze material. Subsequently, the temperature was raised to 1000 °C and maintained for 30 min, followed by a slow cooling down to 700 °C at a ramp rate of 10 °C/min [16]. The power was then disconnected, and the sample was allowed to cool down to room temperature inside the furnace. Ultimately, alumina ceramic floats and pressure-resistant spherical shells with viewing windows were obtained.

2.7. Characterization of Alumina Ceramic Hollow Floating Spheres

The raw ceramic hemispherical shells were obtained by slip casting and the specimens of ceramic hemispherical shells were sintered using a high-temperature muffle furnace (Shanghai Guangshu Electromechanical Co., Ltd., Shanghai, China), increasing the temperature to 350 °C at a rate of 10 °C/min, holding at 350 °C for 1 h for debinding, and then increasing the temperature to 1550~1650 °C at a rate of 5 °C/min holding for 2~8 h. The sintering was completed followed by air cooling to room temperature. The cross-sectional morphology was characterized by field-emission scanning electron microscopy (FESEM, S-4800, Hitachi, Tokyo, Japan).

The cross-sections of the crushed spherical samples were tested by polarized light microscopy (Nikon, E200, Tokyo, Japan), and the wall thickness of the hemispherical shell was measured using vernier calipers. The outer diameter of the sintered ceramic hemispherical shells was measured. The material density of the resulting ceramic sintered hemispherical shells was determined by an electronic balance. The material density of the samples was tested using the Archimedes drainage method. The mass drainage ratio of the ceramic hollow float was calculated by Equation (2), and the buoyancy coefficient B of the ceramic float was calculated by Equation (3) [2]. Buoyancy was measured using deionized water and 4 wt% NaCl solution to simulate seawater. The measured values of the eight spheres were averaged and used for further calculations.

$$\rho = \rho_{water} \frac{m_1}{m_1 - m_2} \tag{1}$$

$$\rho_{sphere} = \frac{m}{v} = \frac{\rho\left(r^3 - (r-t)^3\right)}{r^3} \tag{2}$$

$$\mathrm{B} = \frac{\rho_{water} - \rho_{sphere}}{\rho_{water}} \tag{3}$$

where m_1 is the dry mass of the sample, g; m_2 is the wet weight of the sample, g; ρ_{sphere} is the mass drainage ratio of ceramic hollow sphere, g/cm^3; m is the mass of ceramic hollow sphere, g; r is the radius of hollow sphere, mm; t is the wall thickness of hollow sphere, mm; B is the buoyancy factor of hollow sphere, %; ρ_{water} is the density of water, taken as 0.9965 g/cm^3.

The mechanical properties of brazed joints are characterised by the size of the shear strength of the welded specimen, and the test was carried out using an Instron 5967 universal materials testing machine (Instron Corporation, Norwood, MA, USA) to carry out tensile tests to determine the shear strength of the welded specimen. The beam moved at a loading speed of 1.0 mm/min, and the ceramic material used for the test was a mold identical to the prepared alumina ceramic hemispherical shell, and the specific overlap of the welded specimen is shown in Figure 3. We calculated the shear strength of the joint according to Equation (4)

$$\tau = \frac{F}{S} \tag{4}$$

where τ is the shear strength of the welded joint, MPa; F is the pressure exerted on the alumina ceramic specimen in the experiment, N; S is the contact area of the two alumina ceramic specimens welded together, mm^2.

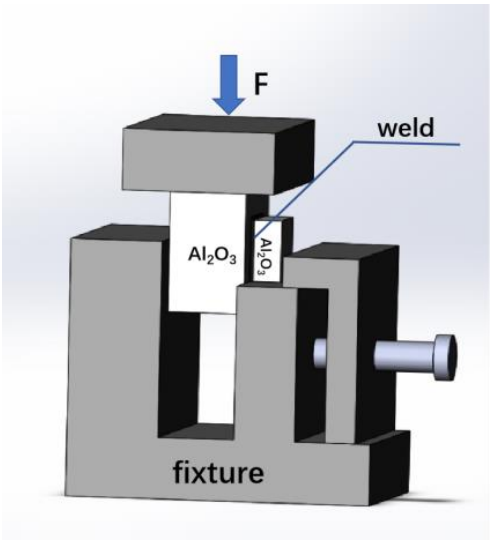

Figure 3. Welded joint shear schematic.

X-ray diffraction (XRD; Empyrean, PANalytical, Almelo, The Netherlands) was used to study the crystal structure, with Cu Kα radiation (λ = 0.154 nm) at 40 kV and 40 mA, in which the grazing angle was set to 0.1°.

A scanning electron microscope (JSM-IT300, Electronics Co., Ltd., Tokyo, Japan) was used to observe the cross-sectional morphology of the sintered body with a minimum magnification of 5000 and a maximum magnification of 100,000, with an accelerating voltage of 20 kV.

The implosion test of the welded ceramic hollow floating balls was conducted in the high-pressure environment laboratory of the National Deep Sea Base Management

Center (NDSCTC-04, Qingdao, China). Thus, 20 welded alumina ceramic hollow floating balls were tested for 8 h of pressure-holding and cyclic pressurization using a 120 MPa hydrostatic test machine (NDSCTC-04, China).

3. Results and Discussion

3.1. Preparation

During the casting process, the ceramic slurry relies on the water absorption of the plaster mold. This causes the water and alumina particles in the slurry near the mold wall to be drawn into the mold, gradually accumulating and thickening to form a thin-walled layer. Once the requirements of the designed specimen are met, the excess slurry is poured out. As the water evaporates, the billet further cures and is demolded to obtain a hemispherical ceramic blank after reaching a certain strength.

3.2. Effect of Solid Content and Dispersant Content on Slurry Viscosity

The viscosity of alumina ceramic slurries is positively correlated with the solid content range. As the solid content increases, the viscosity of the ceramic slurry gradually increases. This perplexing phenomenon occurs because increasing the solid content leads to an increased tendency of aggregation between particles, resulting in an increase in slurry viscosity and a decrease in fluidity. However, elevating the level of solid content in the slurry can significantly improve the strength of both the green body and sintered ceramics. Under conditions where viscosity is less than 1000 mPa·s, the ceramic slurry exhibits high flowability. Therefore, in this experiment, a high-solid-content slurry containing 70 wt% was selected for forming the ceramic hemisphere shell. To further reduce the viscosity of the slurry, a dispersant can be added during slurry preparation. The principle of fluidic slurry dispersion systems lies in the dual-layered charge repulsion mechanism and steric hindrance effect. Long molecule chains act as a spatial obstacle, and surface-bound charges provide electrostatic stabilization effects. The best fluidity performance is achieved when the dispersant content is 0.25 wt%. Thus, a high-solid-content and low-viscosity slurry is critical for shaping high-strength ceramic green bodies.

3.3. Effect of Sintering Temperature on Ceramic Densification

The macroscopic properties of ceramics are determined by their microstructure [26]. The hemispherical ceramic shells, which had been sintered at high temperatures, were crushed and processed in order to screen out the ceramic fragments, and those with a neat cross-section were selected; their cross-section was grinded with silicon nitride abrasive paper on an automatic grinder. After the grinding process, the samples were polished using a 2.5 μm diamond suspension, then ultrasonically cleaned with alcohol, dried in a hot-air oven, and finally micromorphologically observed. Figure 4 illustrates the sectional morphology of ceramic hemisphere shells prepared under different temperature ranges of green compacting and sintering. In Figure 4a, the sectional morphology of the unsintered green compact is depicted, showing numerous small grains with smooth edges and no corners. The aluminum oxide powder remains unsintered at this stage, resulting in a loose structure with a high pore content. Upon increasing the sintering temperature to 1600 °C, as depicted in Figure 4b, the previously small grains undergo significant growth through sintering, resulting in a thorough sintering process. The grain size reaches approximately 10 μm, with uniform size, prominent corners, and some tiny pores. However, further increasing the sintering temperature to 1650 °C, as shown in Figure 4c, leads to abnormally significant growth of large grains. This results in increased gaps between grains and a gradual increase in the number of small pores, which aggregate into larger ones. Finally, at a sintering temperature of 1700 °C, larger grains fuse to form larger agglomerates, and small voids further aggregate into large pores, potentially leading to defects such as cracking or fragmentation of the sintered sample, as depicted in Figure 4d. Therefore, in order to enhance the strength of the ceramic hemisphere shell and the compressive strength of the

ceramic hollow floating ball after welding, the sintering temperature of alumina ceramic in this experiment is set at 1600 °C [27].

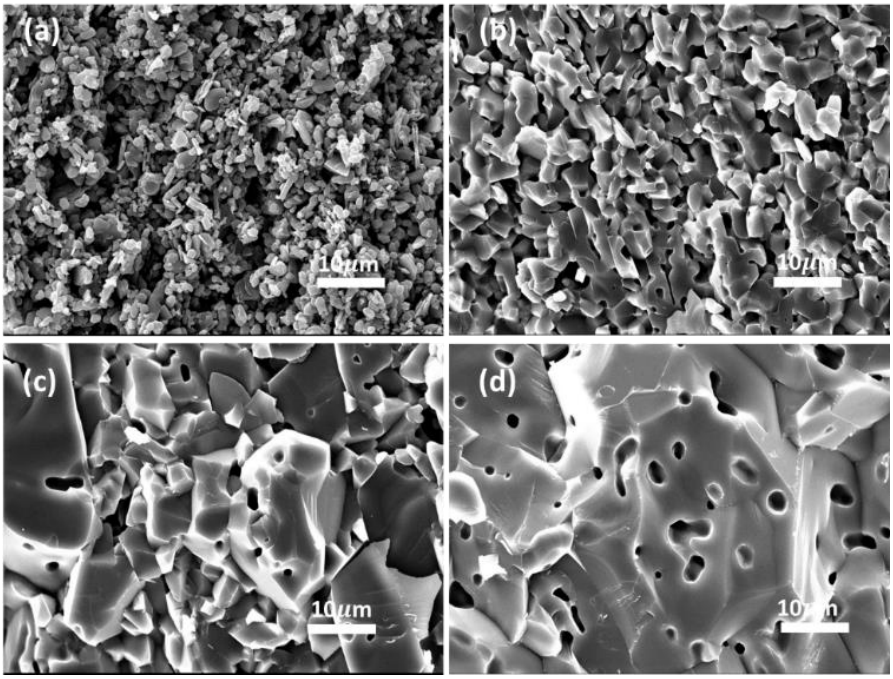

Figure 4. The cross-sectional morphology of ceramic hemispherical shells prepared from raw hemispherical shells and sintered at three temperature intervals. (**a**) The cross-sectional shape of raw unsintered hemispherical shells. (**b**) The section of ceramic hemishell sintered at 1600 °C. (**c**) The cross-section of ceramic hemishell sintered at 1650 °C. Lastly, (**d**) represents the section of ceramic hemishell sintered at 1700 °C.

3.4. Physical Properties of Ceramic Hollow Floating Ball

Varying the deposition time of the ceramic slurry added to the plaster mold allows for the production of different ceramic floating spheres. These spheres possess identical radii and dimensions but exhibit varying wall thicknesses. Upon comparing the morphology and dimensions of the unprocessed hemispherical shells to the sintered hemispherical shells, it is observed that the diameter of the unprocessed hemispherical shells measures 57.14 mm, while the diameter of the sintered shells measures 48.36 mm. The shrinkage of the hemisphere shells is calculated to be 15.3%.

3.5. Aluminum Oxide Ceramic Hollow Float Wall Thickness Measurement

The wall thickness of the produced ceramic hemisphere shells was measured by destructively analyzing them, and the cross-section of the ceramic sphere samples was observed using polarized light microscopy. The wall thickness was then measured using a micrometer. In the raw state, the average wall thickness of the ceramic spheres was determined to be 1.20 mm, while in the sintered state, it measured 1.02 mm, indicating a sintering shrinkage of 15.6% in wall thickness. The sintered spheres exhibit very thin and dense walls, suggesting that the preparation method possesses high molding and sintering properties.

Eight ceramic hemispherical shells were produced using the same process, each numbered separately. The wall thickness of the alumina ceramic hemispherical shells in the sintered state was measured, with measurement points indicated in Figure 5. Specifically, measurements were taken at intervals of every 10° along the latitude. The wall thicknesses of the remaining seven hemispherical shells were measured in both the raw and sintered states.

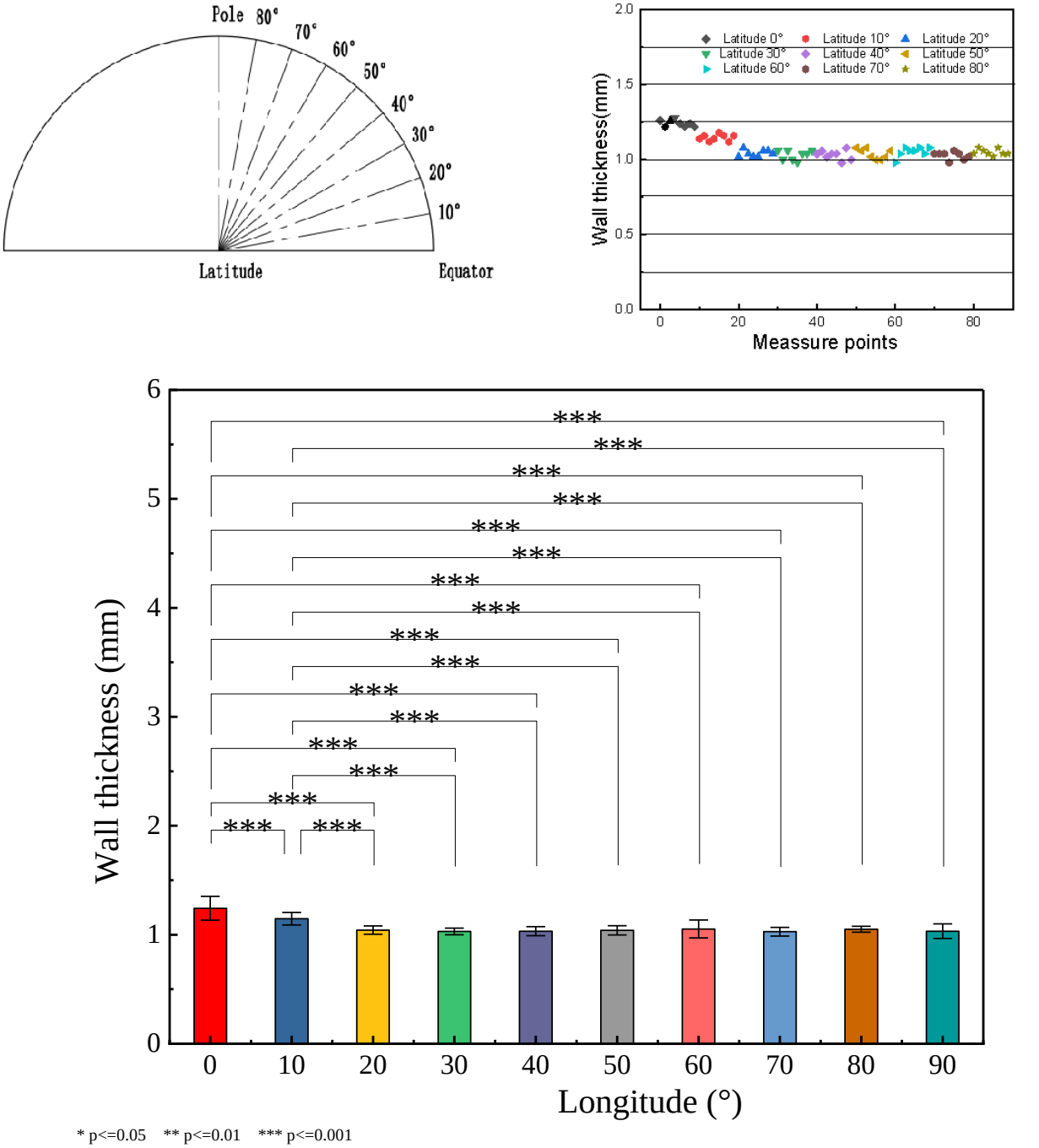

Figure 5. Wall thickness distribution of ceramic hemisphere shell.

3.6. Alumina Ceramic Hollow Float Outside Diameter Measurement

The diameters of the ceramic hollow floating balls were measured on the surface of the fabricated ceramic hollow floating balls in groups of eight, with the measurement points depicted in Figure 6. Specifically, measurements were taken at intervals of every 45° of longitude, resulting in four sets of diameters measured for each hollow floating ball, and the average value was calculated. The average outer diameter of the ceramic hemisphere shell obtained through sintering was determined to be 48.50 mm, slightly exceeding the design value of 48 mm. Similar to the variation in wall thickness, the presence of voids during the preparation process of alumina ceramic hollow floating balls resulted in the final specimen being slightly larger than the theoretical design value.

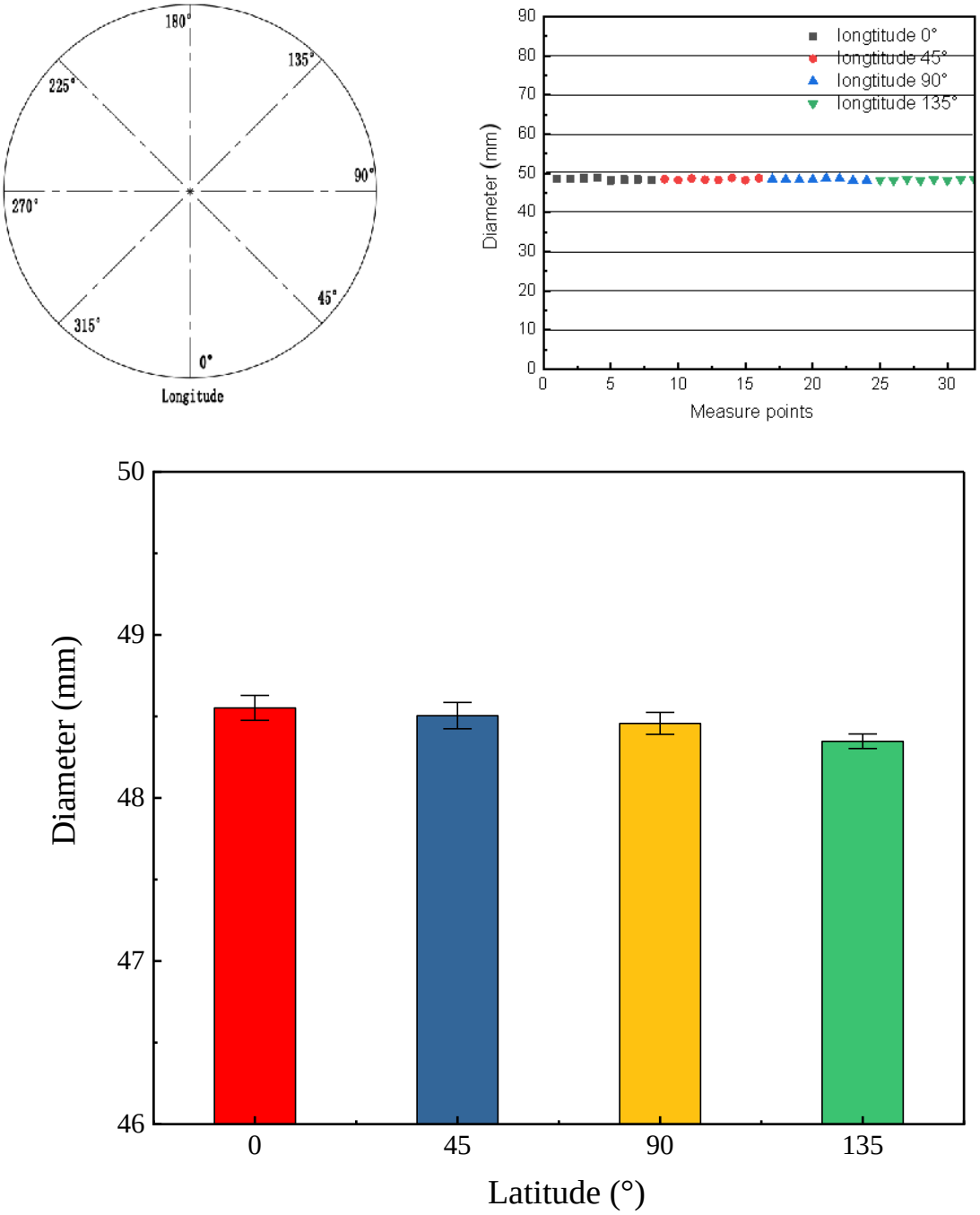

Figure 6. Ceramic hollow float diameter measurement results.

3.7. Mass-to-Water Displacement Ratio and Buoyancy Measurement of Alumina Ceramic Hollow Floats

The material density of alumina ceramic hollow floating spheres was determined using the Archimedes drainage method. Initially, the sample underwent drying in an oven, and its dry weight m_1 was recorded. Subsequently, the sample was placed in a beaker within a vacuum system, and water was introduced into the beaker while maintaining a vacuum to facilitate water penetration into the sample's pores under negative pressure. After removal from the vacuum system, the sample's surface moisture was wiped off with a damp cloth, and its wet weight m_2 was measured. Additionally, the material density of eight sintered ceramic hemispheres was measured. The average density of the sintered

hemispheres was found to be 3.83 g/cm^3, representing 98.1% of the density of the alumina material, thus demonstrating the superior quality of the sintered hemispheres.

The measured density of the sintered hemispherical shell sample was used to calculate the mass drainage ratio and buoyancy coefficient of the ceramic hollow float obtained after welding, as per Equations (2) and (3). The mass drainage ratio of the ceramic hollow float was determined to be 0.467 g/cm^3, with a corresponding buoyancy coefficient of 53.36%. These values were then compared with those of the conventional ceramic float, which typically has a mass-to-drainage ratio of 0.72 g/cm^3 [28,29]; the ceramic float prepared through this process demonstrates a significantly enhanced buoyancy capability (Table 1).

Table 1. Ceramic hollow ball mass-to-drainage ratio.

Number	Dry Weight/g	Wet Weight/g	Material Density (g/cm^3)	Mass-to-Drainage Ratio/(g/cm^3)
1	14.480	10.666	3.810	0.463
2	15.246	11.243	3.822	0.471
3	14.865	10.968	3.828	0.468
4	13.764	10.162	3.834	0.462
5	13.868	10.244	3.840	0.466
6	14.246	10.513	3.830	0.470
7	14.620	10.795	3.836	0.465
8	15.166	11.180	3.818	0.472
Average	14.532	10.721	3.827	0.467
SD	0.171	0.167	0.032	0.005

3.8. Performance Parameters of Hollow Spheres

The measurement results summarised above provide an overview of the performance of hollow floating spheres formed from welded ceramic hemispherical shells (Table 2). The ceramic hollow floating ball, with a sintered wall thickness of 1.00 mm and a diameter of 48.52 mm, exhibited a material density of 3.827 g/cm^3. Additionally, the mass drainage ratio was recorded as 0.467 g/cm^3, while the buoyancy coefficient stood at 53.36%.

Table 2. Ceramic hollow ball performance parameters.

Performance	Results
Material density, g/cm^3	3.827 ± 0.032
Relative density	98.20 ± 0.09
Mass, g	29.24 ± 0.12
Wall thickness, mm	1.02 ± 0.02
Diameter, mm	48.52 ± 0.16
Mass to drainage ratio, g/cm^3	0.467 ± 0.005
Buoyancy factor, %	53.36 ± 0.38

3.9. Effect of Welding Temperature and Brazing Material Composition on the Welding Performance of Alumina Ceramic Floating Balls

To explore the welding performance of ceramic hollow floating balls, a series of alumina ceramic test strips were cast and shaped using an identical procedure. The optimal welding temperature for enhanced performance was determined by analyzing the shear strength of the welded joints of these test strips.

Figure 7 illustrates the joint strength at various temperatures based on the shear strength test results. The findings indicate that at a connection temperature of 900 °C, the joint strength is the lowest at only 30.2 MPa. Subsequently, as the connection temperature increases to 950 °C, the shear strength rises to 45.8 MPa. Upon further elevation of the temperature to 1000 °C, the shear strength peaks at 62.3 MPa before declining with continuing temperature increases. This phenomenon can be attributed to the significant influence of temperature on the sintering process, particularly on the dissolution of the solder. From room temperature to 900 °C, the brazing material on the welded contact surface undergoes

incomplete decomposition due to insufficient heat, resulting in only partial welding of the contact surface and a subsequent decrease in joint strength. At 950 °C, the whiskers formed at the interface are excessively fine. However, at 1000 °C, complete dissolution of the brazing material reinforces the joint interface. Nevertheless, further temperature elevation leads to increased whisker adhesion and decomposition, ultimately diminishing the strength of the joint.

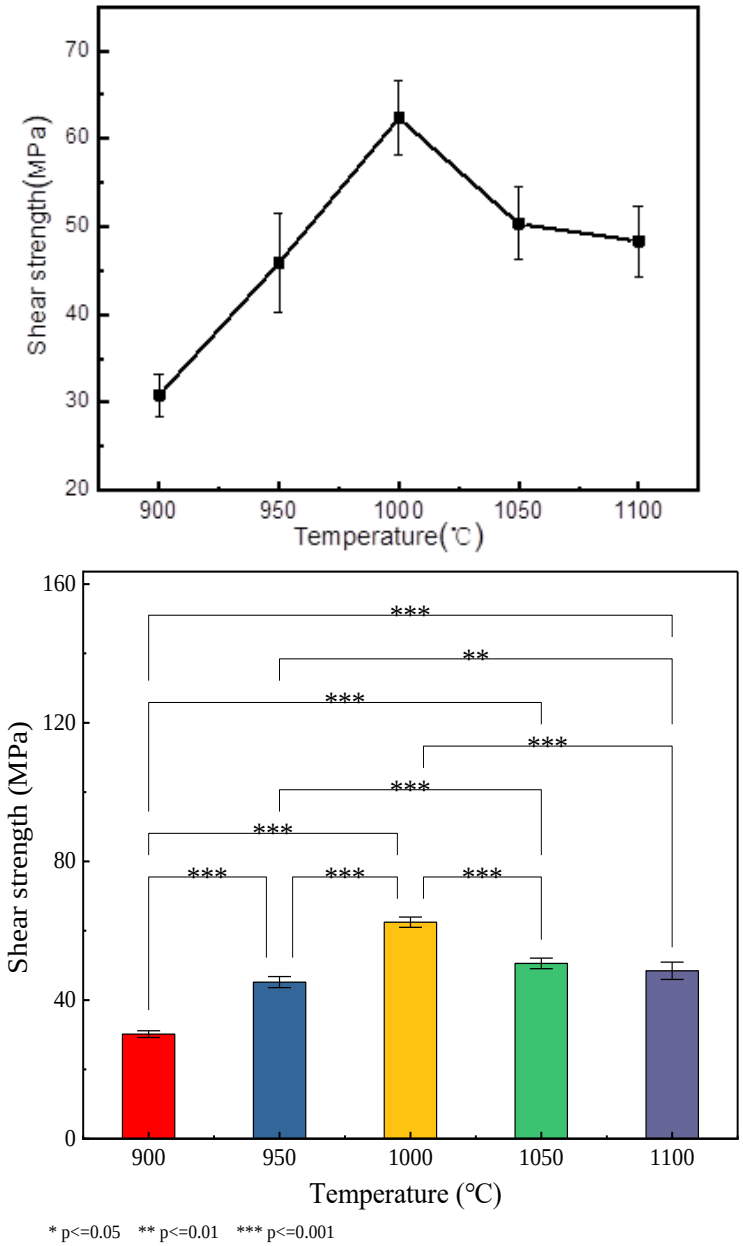

Figure 7. Shear strength versus brazing temperature.

Figure 8 displays the XRD results. The analysis reveals that the primary phases present at the metal braze and Al_2O_3 ceramic welds include Al_2O_3, Ag, CuO, and others. Al_2O_3 and Ag represent the principal constituents of the base material and the metal brazing material, respectively. XRD analysis further indicates complete dissolution of the brazing material at a welding temperature of 1000 °C. At this temperature, the weld exhibits the highest CuO content. Moreover, CuO enhances the wetting ability of the Ag-Cu eutectic metal braze on Al_2O_3 ceramics [30,31].

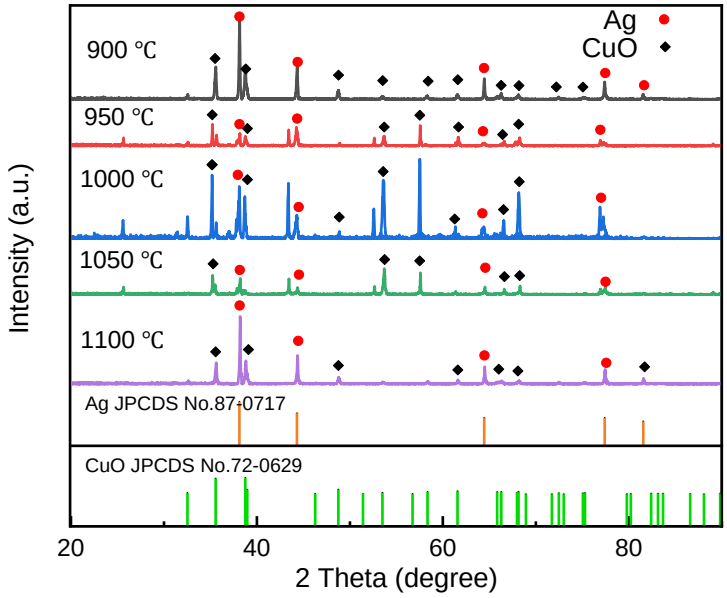

Figure 8. X-ray diffraction analysis results of the weld interface phase.

The introduction of CuO powder successfully enhanced the wetting capability of the Ag-Cu eutectic metal braze on Al_2O_3 ceramics. To further enhance the performance of ceramic welding, different proportions of CuO powder were added to the Ag-Cu eutectic metal brazing material as a percentage of the total brazing material mass fraction, thus creating a new metal brazing material. Figure 9, presenting the shear strength test results, indicates that at a constant brazing temperature, the overall effect of CuO addition on joint strength follows an initial increase followed by a decreasing trend. This phenomenon occurs because, within a specific range, an increase in the CuO addition enhances the wetting capability of the brazing material on the Al_2O_3 ceramic surface, thereby facilitating interfacial bonding and elevating the shear strength of the joint. However, CuO constitutes a brittle phase within the bonding interface layer; hence, excessive addition of CuO leads to a reduction in the shear strength of the brazed joint due to an abundance of CuO particles at the interface between the brazing metal and the Al_2O_3 ceramic [32,33].

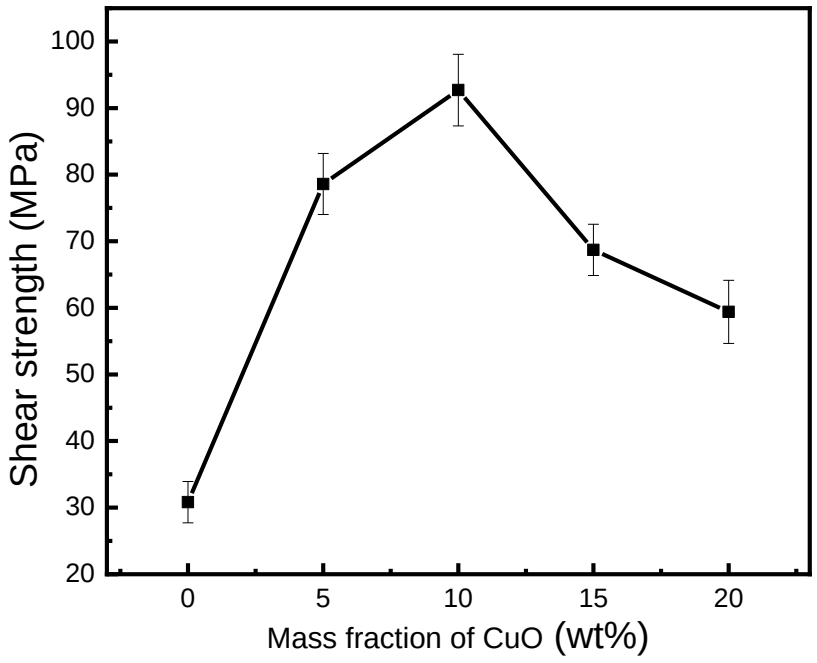

Figure 9. *Cont.*

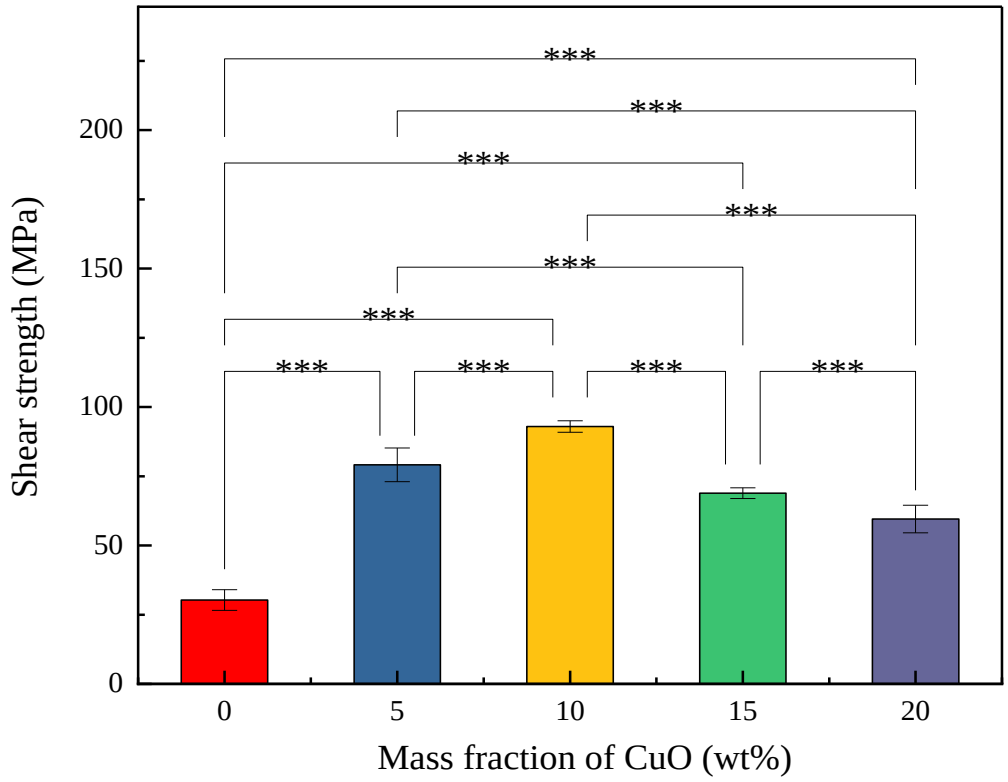

Figure 9. Relationship between shear strength and CuO content.

3.10. Deep-Sea Pressure Resistance of Alumina Ceramic Hollow Floating Balls

The deep-sea pressure resistance experiments on alumina ceramic hollow floating spheres were carried out in the high-pressure environment laboratory at the National Center for Deep Sea Base Management. Two experiments were conducted to assess the pressure resistance of the ceramic hollow floating balls. One method involved subjecting a batch of floating balls to a specific, sustained pressure at a certain water depth over an extended duration. Alternatively, another experiment involved rapidly cycling the pressure up and down multiple times within a shorter period for the same batch of floating balls. The performance of the experimental ceramic floats was evaluated to ascertain the deep-sea pressure resistance of the prepared alumina ceramic hollow floats [34,35].

In this study, twenty alumina ceramic hollow floats were prepared for testing in an environment simulating real seawater conditions for deep-sea operations. Ten of these floats underwent an ultimate compressive strength test, subjected to a pressure of 120 MPa, with a ramp-up rate of 10 MPa/min, an 8 h holding pressure, and a ramp-down rate of 10 MPa/min. The results of the holding pressure fatigue test are presented in Figure 10.

The remaining ten floats were utilized for cyclic pressurization tests, with a ramp-up speed of 10 MPa/min, reaching a pressure of 100 MPa, holding pressure for 10 min, and then ramping down at a speed of 10 MPa/min to 0 for one cycle. The total number of cycles conducted was 100. Since the ultimate compressive strength of the machine was limited to 120 MPa, the ten tested floats remained intact without damage, demonstrating excellent performance under 120 MPa. The cyclic pressure fatigue test results are detailed in Figure 11, where all samples completed the test without incurring any damage.

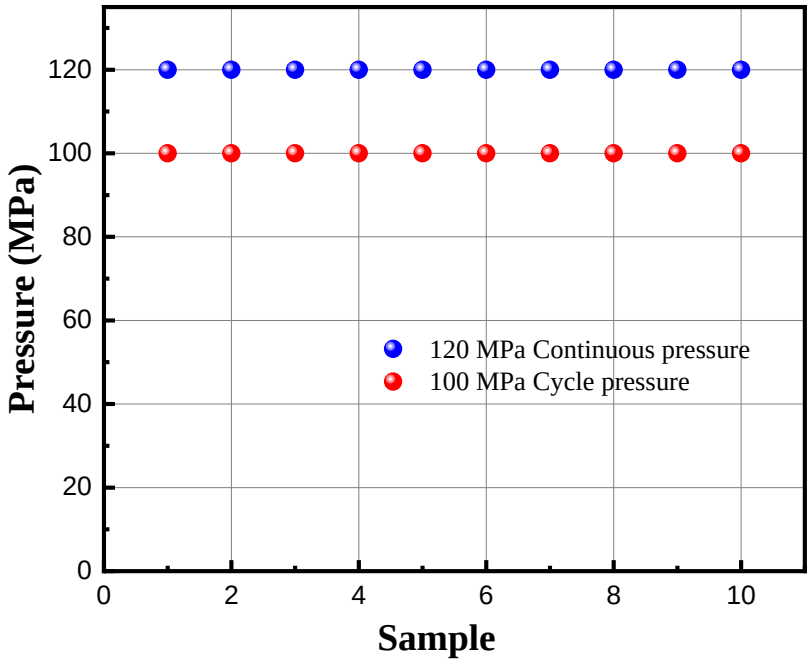

Figure 10. Cyclic compressive strength test and continuous compressive strength test.

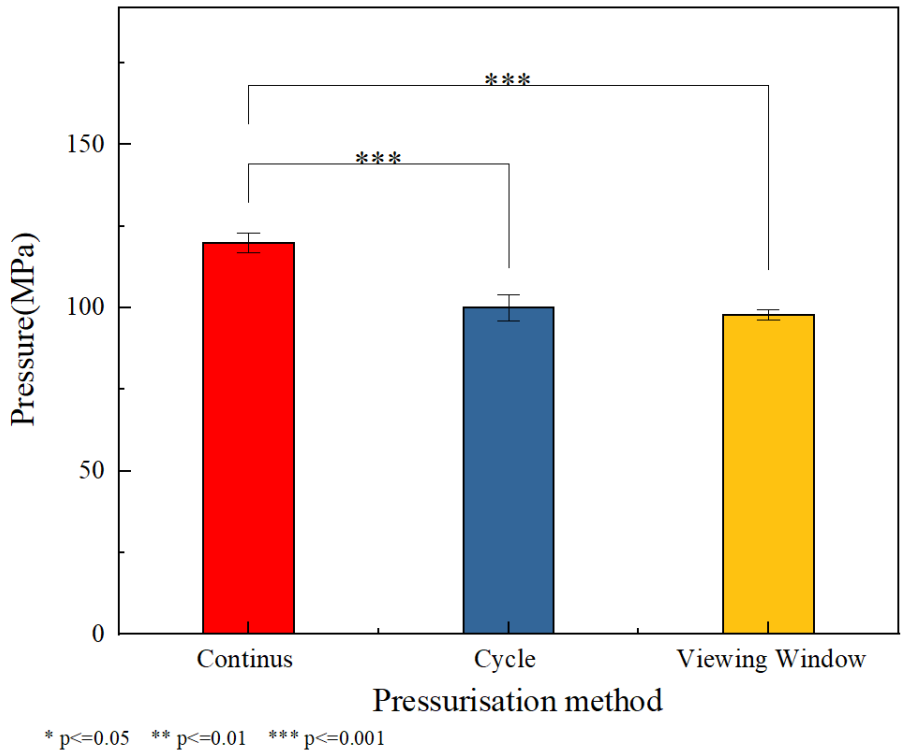

Figure 11. Float pressure resistance test with observation window.

4. Conclusions

The successful large-scale production of deep-sea pressure-resistant ceramic hollow float balls can be achieved through an innovative and practical approach. Unlike the conventional method of directly forming seamless whole spheres, this approach involves the preparation of ceramic half-spheres using the traditional casting method with sedimentation. This sedimentation process yields semi-spherical shell specimens with uniform wall thickness, which is critical for the mechanical integrity of ceramic balls. By employing a method to weld two half-shell components together, the surface of each half-shell com-

ponent is processed, significantly enhancing the production efficiency of ceramic hollow float balls while increasing the product yield rate. Furthermore, the material density of the half-spherical shell samples was measured, resulting in a density of 3.827 g/cm^3, confirming the quality of the alumina material at 98.20% of its density. Measurements of the wall thickness of the ceramic hollow sphere formed by welding alumina ceramic half-spheres revealed a thickness of 1.00 mm and a diameter of 48.52 mm, with a mass displacement ratio of 0.467 g/cm^3 and a buoyancy coefficient of 53.36%. Mechanical performance tests demonstrated that the ceramic hollow spheres produced using this process could withstand pressure tests of up to 120 MPa. In continuous and cyclic fluid hydrostatic tests, all tested floating balls exhibited excellent performance without any failures. The advancement of the welding process and the cost-effectiveness and superior properties of alumina materials offer a solution for the subsequent production of larger-sized alumina ceramic floats with improved performance. Additionally, ceramic pressure-resistant spherical shells with open-top ends can be prepared using the slip casting method, with ceramic connectors welded to serve as observation window seats on the spherical shells. These connectors can accommodate glass for external environment observation and can also serve as channels for carrying items needed for deep-sea research or transporting researchers, thereby providing valuable insights for the subsequent use of ceramic pressure-resistant spheres to transport people and items.

Author Contributions: Y.L.: Investigation, experimental design, sample preparation, data management, validation, and writing the original draft. J.Z.: Investigation, project management, manuscript editing, manuscript revision. G.L.: Investigation, project management, sample testing. L.W.: Investigation, experimental design, Z.D.: Sample testing. All authors have read and agreed to the published version of the manuscript.

Funding: The authors thank the Key R&D Program of Shandong Province (2020JMRH0101) for the financial support of this work.

Data Availability Statement: Data are contained within the article.

Conflicts of Interest: The authors declare no conflict of interest.

References

1. Xu, X.Q.; Wang, X.B.; Wu, S.Y.; Yan, L.C.; Guo, T.; Gao, K.W.; Pang, X.L.; Volinsky, A.A. Design of Super-Hard High-Entropy Ceramics Coatings Via Machine Learning. *Ceram. Int.* **2022**, *48*, 32064–32072. [CrossRef]
2. Rastogi, V.K.; Sturzenegger, P.N.; Gonzenbach, U.T.; Vetterli, M.; Naikade, M.; Kesari, K.K.; Ruokolainen, J.; Kuebler, J.; Blugan, G. High Precision Pulp-Based Sacrificial Molds: A Solution Towards Mass Production of Hollow Ceramic Spheres for Deep Sea Applications. *Ceram. Int.* **2022**, *48*, 8235–8244. [CrossRef]
3. Qi, H.; He, C.G.; Zhang, P.Z.; Han, W.Y.; Guo, F.Q.; Wu, F.; Du, M.F. Additive Manufacturing of Silicon Nitride Ceramic Floatation Spheres with Excellent Mechanical Properties. *Materials* **2019**, *12*, 2717. [CrossRef] [PubMed]
4. Biswas, P.; Mamatha, S.; Naskar, S.; Rao, Y.S.; Johnson, R.; Padmanabham, G. 3D Extrusion Printing of Magnesium Aluminate Spinel Ceramic Parts Using Thermally Induced Gelation of Methyl Cellulose. *J. Alloys Compd.* **2019**, *770*, 419–423. [CrossRef]
5. Wang, C.P.; Wang, S.H.; Wang, H.Z.; Ruan, G.L.; Xiao, Y.X.; Jiang, Z.G.; Li, X.P. Research Status and Prospects of Tribological Behaviors of Key Friction Pairs of Materials in Marine Equipment. *Mater. Sci.* **2021**, *27*, 148–154. [CrossRef]
6. Zhang, K.T.; Xu, Y.; Chen, L.G.; Fu, L.; Jia, S.K.; Zhao, Z.G. Effect of Aluminum Chloride Addition on the Crystal Structure, Micromorphology, Dielectric Properties, and Ferroelectric Properties of BZT Ceramic. *Glass Ceram.* **2022**, *78*, 506–511.
7. Li, S.; Zhang, Y.; Han, J.; Zhou, Y. Fabrication and Characterization of SiC Whisker Reinforced Reaction Bonded Sic Composite. *Ceram. Int.* **2013**, *39*, 449–455. [CrossRef]
8. Gong, Y.; Tian, W.; Zhang, P.; Chen, J.; Zhang, Y.; Sun, Z. Slip Casting and Pressureless Sintering of Ti_3AlC_2. *J. Adv. Ceram.* **2019**, *8*, 367–376. [CrossRef]
9. Cho, K.S.; Kim, J.; Lee, S.Y.; Oh, J.P.; Park, S.I. Shape Forming of Alumina by Step Pressure-Vacuum Hybrid Slip Casting. *Appl. Mech. Mater.* **2012**, *217*, 1899–1902. [CrossRef]
10. Ndinisa, S.S.; Whitefield, D.J.; Sigalas, I. Fabrication of Complex Shaped Alumina Parts by Gelcasting on 3D Printed Moulds. *Ceram. Int.* **2020**, *46*, 3177–3182. [CrossRef]
11. Gorman, J.; Parry, J. The Opportunity of Modern High-Toughness Technical Ceramics for Undersea Systems. *Mar. Technol. Soc. J.* **2021**, *55*, 50–55. [CrossRef]
12. Gizowska, M.; Konopka, K.; Szafran, M. Properties of Water-Based Slurries for Fabrication of Ceramic-Metal Composites by Slip Casting Method. *Arch. Metall. Mater.* **2011**, *56*, 1105–1110. [CrossRef]

13. Zhang, Y.; Chen, Y.; Yu, D.; Sun, D.; Li, H. A Review Paper on Effect of the Welding Process of Ceramics and Metals. *J. Mater. Res. Technol.* **2020**, *9*, 16214–16236. [CrossRef]
14. Benedetti, A.; Gambaro, S.; Valenza, F.; Faimali, M.; Colli, M.; Hostaša, J.; Delucchi, M. Ag and Agcu as Brazing Materials for Ti_6Al_4V-$Y_3Al_5O_{12}$ Joints: Does Ennoblement Affect the Galvanic Behaviour in Seawater? *Electrochim. Acta* **2018**, *283*, 155–166. [CrossRef]
15. Zhang, J.; Zhang, J.; Li, L.; Zhang, C.; Zhang, Y.; Lu, X. Stress Analysis of the Brazing Joints of Tubular Ceramic Oxygen-Permeable Membranes and Metal Supports. *Ceram. Int.* **2019**, *45*, 1545–1553. [CrossRef]
16. Li, Y.X.; Chen, C.; Yi, R.X.; He, L.Z. The Brazing of Al_2O_3 Ceramic and Other Materials. *Int. J. Adv. Manuf. Technol.* **2022**, *120*, 59–84. [CrossRef]
17. Marulcuoglu, H.; Kara, F. Microstructure and Mechanical Properties of Dense Si_3N_4 Ceramics Prepared by Direct Coagulation Casting and Cold Isostatic Pressing. *Mater. Sci. Eng. A* **2022**, *854*, 143782. [CrossRef]
18. Wang, F.; Wang, M.Q.; Wang, W.W.; Yang, L.; Zhang, X.Z. Time-Dependent Axial Displacement of Pmma Frustums Designed for Deep-Sea Manned Cabin Based on Finite Element Analysis. *Ships Offshore Struct.* **2021**, *16*, 827–837. [CrossRef]
19. Wang, N.; Chang, H.; Zhang, C.; Wu, Y.N.; Yang, R.; Zhang, X.; Zhai, Z.R. Preparation of High-Stability Ceramic Slurry with Gel Behavior for Stereolithography 3D Printing. *Materials* **2023**, *16*, 2816. [CrossRef]
20. Cao, Y.; Xu, G.C.; Shen, P. Flash Joining of 3YSZ and 430 SS Using Ag-CuO Filler. *Ceram. Int.* **2022**, *48*, 4005–4014. [CrossRef]
21. Sun, S.; Zhao, M. Numerical Simulation and Analysis of the Chain-Reaction Implosions of Multi-Spherical Hollow Ceramic Pressure Hulls in Deep-Sea Environment. *Ocean Eng.* **2023**, *277*, 114247. [CrossRef]
22. Wu, Y.; Luo, R.; Wang, F.; Zhao, M.; Xia, J. Effect of the Implosion of a Deep-Sea Pressure Hull on Surrounding Structures. *Appl. Ocean Res.* **2023**, *132*, 103477. [CrossRef]
23. Wang, P.; Wang, Y.H.; Yang, S.Q.; Niu, W.D.; Wang, X.H.; Li, P.H. Analysis, Simulation and Experimental Study of the Tensile Stress Calibration of Ceramic Cylindrical Pressure Housings. *J. Mar. Sci. Eng.* **2022**, *10*, 499. [CrossRef]
24. Liu, X.; Wu, Q.Q.; Yu, G.C.; Wu, L.Z. Failure Behavior of the Ceramic Thin-Walled Cylindrical Shell under the Hydrostatic Pressure. *Compos. Struct.* **2022**, *295*, 115828. [CrossRef]
25. Naidich, Y.V.; Gab, I.I.; Stetsyuk, T.V. Brazing Oxide Ceramics Via the Ductile Interlayers of Niobium and Noble Metals. *Powder Metall. Met. Ceram.* **2016**, *55*, 454–457. [CrossRef]
26. Liu, Y.Y.; Wang, C.Y.; Zhang, K.D. Laser Sintering of Al_2O_3-Based Green Ceramics Prepared by Different Pre-Sintering Temperatures. *Int. J. Appl. Ceram. Technol.* **2022**, *19*, 1904–1915. [CrossRef]
27. Liu, Z.Y.; Xie, N.; Zhang, H.X.; Huang, S.W.; Wu, C.M.; He, S.H.; Zhu, J.B.; Liu, Y. Effect of $Al(OH)_3$ Addition on Densification Mechanism and Properties of Reaction-Sintered Mullite-Corundum Composite Ceramics. *J. Asian Ceram. Soc.* **2022**, *10*, 703–712. [CrossRef]
28. Dong, X.; Wang, M.C.; Tao, X.; Liu, J.C.; Guo, A.R. Properties of Heat Resistant Hollow Glass Microsphere/Phosphate Buoyancy Materials with Different Coatings. *Ceram. Int.* **2020**, *46*, 415–420. [CrossRef]
29. Zheng, B.; Zhuang, M.M.; Guo, A.R.; Wang, M.C.; Ren, S.E.; Geng, H.T.; Liu, J.C. Buoyancy Materials of Aluminium Borosilicate Glass for High Temperature Resistance. *Mater. Res. Innov.* **2015**, *19*, S50–S53. [CrossRef]
30. Kaur, J.; Khanna, A.; Kumar, R.; Chandra, R. Growth and Characterization of Cu_2O and CuO Thin Films. *J. Mater. Sci. Mater. Electron.* **2022**, *33*, 16154–16166. [CrossRef]
31. Wang, X.; Li, C.; Du, Q.; Zhou, Q.; Qi, J.; Si, X.; Cao, J. Brazing Zta Ceramic and Ti_6Al_4V Alloy Directly in Air: Excellent Oxidation Resistance at 800 Degrees C. *Ceram. Int.* **2022**, *48*, 9631–9639. [CrossRef]
32. Zhou, W.L.; Hu, S.P.; Yang, M.J.; Luo, Y.; Fu, W.; Song, X.G. Reactive Air Brazing of 3YSZ Ceramic to Aluminized Crofer22H Stainless Steel Using Ag-CuO Fillers. *Int. J. Appl. Ceram. Technol.* **2022**, *19*, 2367–2378. [CrossRef]
33. Rai, R.S.; Bajpai, V. Improvement of Interfacial Adhesion of CuO Nanostructured Carbon Fiber Reinforced Polymer Composites. *Polym. Compos.* **2023**, *44*, 1789–1804. [CrossRef]
34. Le Gall, M.; Choqueuse, D.; Le Gac, P.Y.; Davies, P.; Perreux, D. Novel Mechanical Characterization Method for Deep Sea Buoyancy Material under Hydrostatic Pressure. *Polym. Test.* **2014**, *39*, 36–44. [CrossRef]
35. Takahashi, K.; Kawabata, Y.; Kobayashi, M.; Gotoh, S.; Nomura, S.; Kasaya, T.; Iwanami, M. Action of Hydraulic Pressure on Portland Cement Mortars—Current Understanding and Related Progress of the First-Ever in-Situ Deep Sea Tests at a 3515 m Depth. *J. Adv. Concr. Technol.* **2021**, *19*, 226–239. [CrossRef]